Hindawi Publishing Corporation
Science and Technology of Nuclear Installations
Volume 2010, Article ID 517471, 8 pages
doi:10.1155/2010/517471

Research Article

Fluid-Structure Interaction in a 3-by-3 Reduced-Scale Fuel Assembly Network

Guillaume Ricciardi,[1,2] Sergio Bellizzi,[2] Bruno Collard,[1] and Bruno Cochelin[2]

[1] *CEA CADARACHE DEN/DTN/STRI/LHC, 13108 Saint-Paul-Lez-Durance Cedex, France*
[2] *LMA CNRS, 31 chemin Joseph Aiguier, 13402 Marseille Cedex 20, France*

Correspondence should be addressed to Guillaume Ricciardi, guillaume.ricciardi@cea.fr

Received 3 August 2010; Accepted 1 October 2010

Academic Editor: Eugenijus Ušpuras

We present experimental results on 9 reduced-scale fuel assemblies arranged in a network of 3 by 3, subjected to an axial flow. The objective is to analyse the fluid force induced by the motion of the central fuel assembly on the others fuel assemblies. The displacement of the central fuel assembly is imposed, while the others are fixed. Fluid forces acting on fuel assemblies are measured with force sensors. We observed that the coupling between fuel assemblies increases with the fluid velocity, and that the coupling in the transverse direction is not negligible compared to the coupling in the direction of excitation. We also observe that the fluid flow induces a stiffening of the central fuel assembly.

1. Introduction

The safety of a nuclear power plant subjected to a seismic loading is a major concern of the nuclear industry. Engineers need efficient modelling and accurate knowledge of the mechanical behaviour of the reactor core to estimate the effect of an earthquake on a nuclear power plant. The study presented here deals with the Pressurized Water Reactor (PWR) technology. A reactor core is a complex structure consisting of about 150 fuel assemblies side by side in the reactor core case. Each fuel assembly is composed of 289 regularly spaced fuel rods. Each rod is about 1 cm in diameter, 4 m in length, and the gap between two rods is about 2 mm wide (Figure 1). There are two types of rods: 25 guide tubes support the other 264 fuel rods that contain enriched uranium. The guide tubes are welded to 10 regularly spaced grids holding fuel rods. The contact points between grids and fuel rods are fitted with springs, so that the fuel rods can slip into the grids. The fuel assemblies are immersed in pressurized water ($\approx$15 MPa). The fluid flow is mainly axial; the transversal component ($\approx$0.3 m/s) is small in comparison to the axial component ($\approx$5 m/s). Since the fluid velocity is about 5 m/s, the flow is highly turbulent with a Reynolds number of Re = 500 000 at 300°C.

Many studies provide modelling and experimental results of a row of fuel assemblies [1–4], and some proposed 3D modelling [5–7], but there is a lack of 3D experiments presenting not only a row of fuel assemblies but a 3D network. The assumption, usually done according to which behaviour of each row of fuel assemblies is independent of the others, obviously induces some error margin. There is a need to know how important the coupling between two rows of fuel assemblies is, to estimate the error margin. The point is to know if the error is small enough to ensure that 2D simulations are sufficient, or if we need to perform 3D simulations to optimize the fuel assembly design. In this paper, we propose to provide some experimental results on 9 reduced-scale fuel assemblies arranged in a network of 3 by 3, subjected to an axial flow. The objective is to analyse the fluid force induced by the motion of the central fuel assembly on the others fuel assemblies. Moreover, these experimental results will be useful for the validation of numerical modelling simulating the response of a PWR under seismic loading. The displacement of the central fuel assembly is imposed, while the others are fixed, fluid

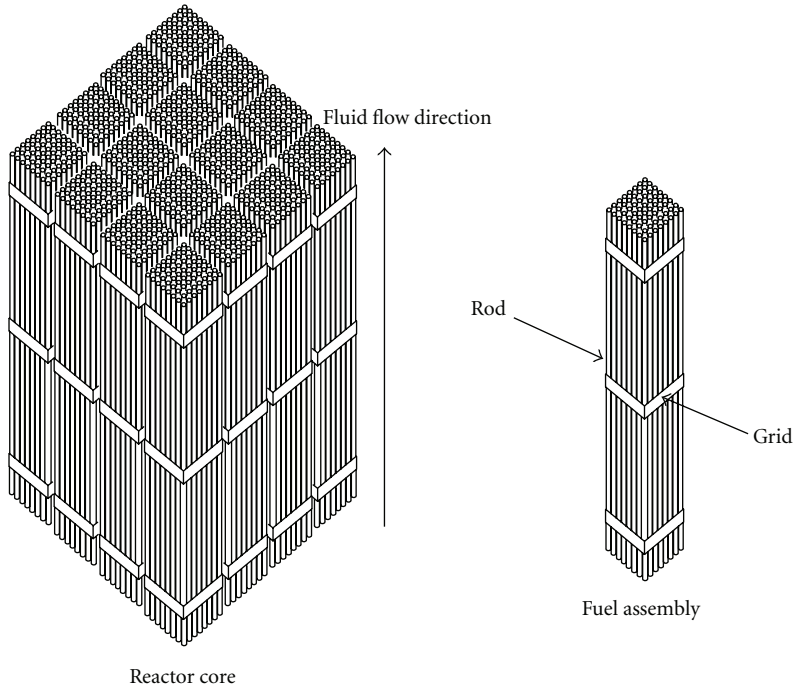

Figure 1: Part of a reactor core (left), part of a fuel assembly (right).

forces acting on fuel assemblies are measured with force sensors.

2. Experimental Apparatus

2.1. Fuel Assemblies. The test section presents 9 reduced-scale fuel assemblies, arranged in a 3-by-3 network surrounded by a frame and subjected to an axial flow inside the frame (Figure 2). Each fuel assembly is made up of 16 fuel rods (network 4 by 4), which are 2.5 m long, for a diameter of approximately 1 cm, and maintained by one grid (at the middle) and two nozzles (Figure 3). The grid is glued, while top and bottom nozzles are screwed to the fuel rods, so that there is no relative displacement and therefore no friction between rods and grids, in order to have fuel assemblies with a linear behaviour.

The gap between assemblies is 5 mm wide, while the width of the grid is 54 mm; areas of pure fluid therefore occupy a significant share of total volume. The assemblies' upper nozzles are screwed to the upper core plate, while linkage with the lower core plate is ensured by centering devices, so that fuel assemblies are clamped-clamped.

The 8 fuel assemblies surrounding the central fuel assembly are fixed at the frame by mean of 8 fastening rods, oriented in the ($\mathbf{e_z}$) direction, connected to the grids of the fuel assemblies. The fastening rods, connected to the three middle fuel assemblies, cross the board fuel assemblies (Figure 3). It should be noted that, the motion of the fastening rod through the board fuel induces a friction force, in spite of precautions taken to prevent this phenomenon.

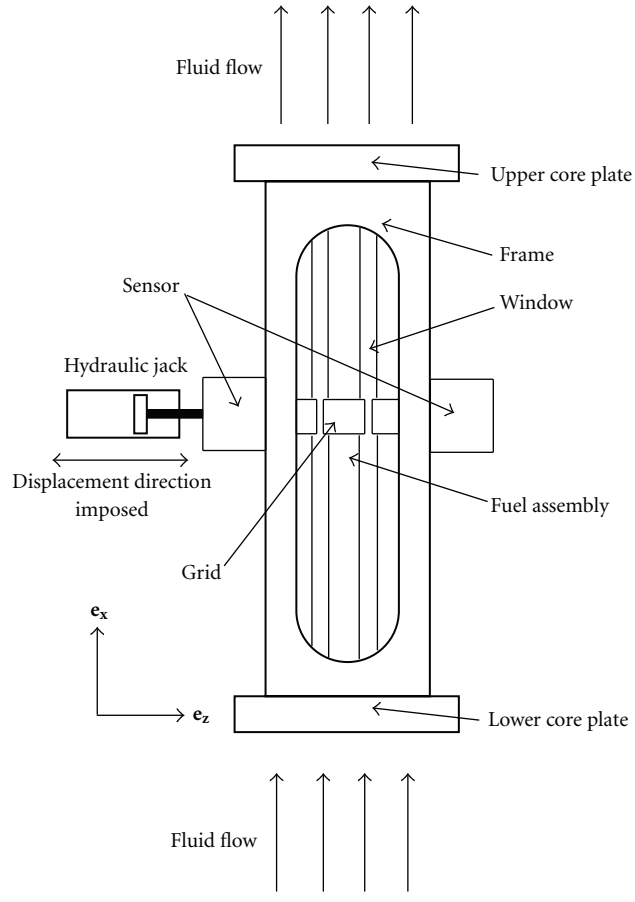

Figure 2: Experimental apparatus.

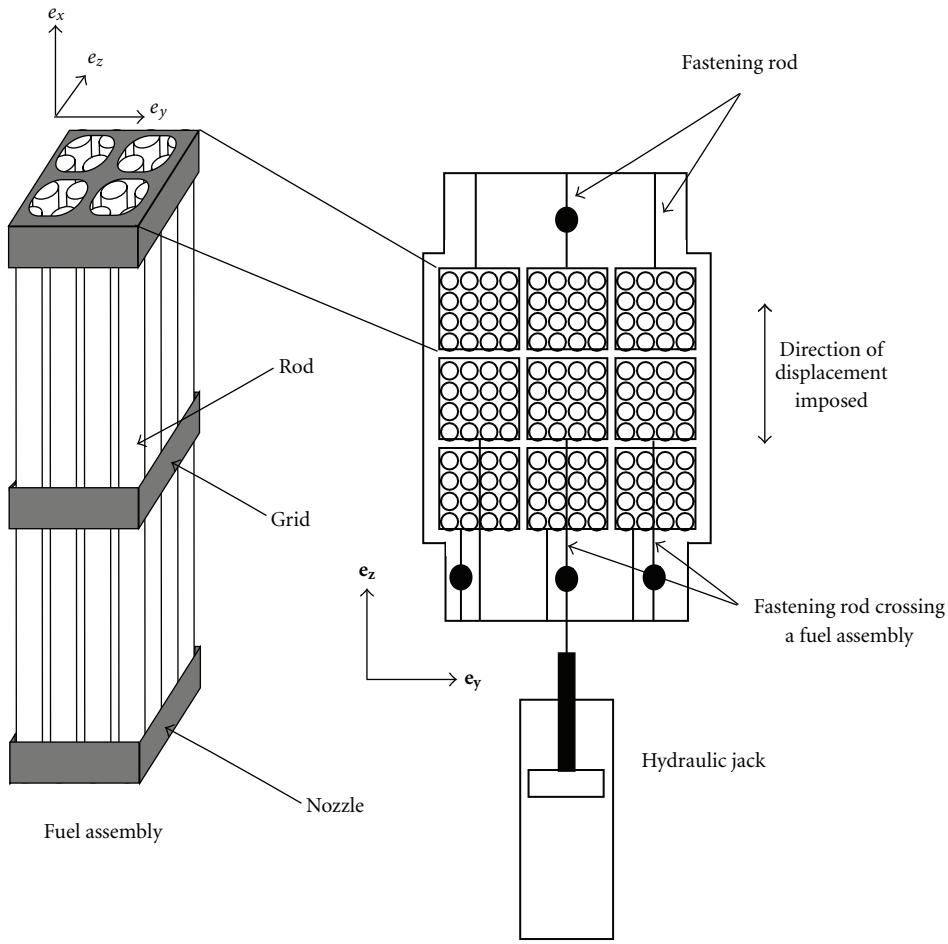

Figure 3: Experimental apparatus (top view).

2.2. External Excitation. A hydraulic jack is connected to the central fuel assembly through a fastening rod, that allows it to impose the displacement of the central assembly grid, in the ($\mathbf{e_z}$) direction, while the other fuel assemblies remain motionless.

A variable speed pump generates the fluid flow in the test loop. The pump allows us to reach the value of around 5 m/s, which is close to the PWR operating condition.

The apparatus allows us to perform static, quasistatic, and dynamic tests, in-air, in still water and under axial flow. The quasistatic tests are performed at a constant velocity of 1 mm/s, imposed on the central fuel assembly. The dynamics tests are carried out for several fluid velocities (from 0 m/s to 4.9 m/s). The movement imposed on the central fuel assembly (noted $\mathbf{u_{central}(t)}$) is a swept sine ranging from 0 Hz to 4 Hz. The fuel assemblies resonant frequency is located at around 2.5 Hz

$$\mathbf{u_{central}(t)} = a_0 \sin\left(\frac{\pi(f_S - f_I)}{T_s} t^2 + 2\pi f_I t\right)\mathbf{e_z}, \qquad (1)$$

where $a_0 = 2$ mm is the magnitude, $f_I = 0$ Hz, $f_S = 4$ Hz, and $T_s = 300$ s is the duration of the scan. All tests were recorded at a 2 kHz sampling frequency.

The limit of 4 Hz is imposed by the sensor linked to the central assembly, indeed beyond this frequency, the force acting on the sensor becomes too high and may exceed the limit of 100 N.

2.3. Measurement. Four strain gauges force sensors are mounted on some fastening rods (Figure 4). The two spherical linkages (Figure 5) ensure that the sensors are only subjected to a tensile force in the $\mathbf{e_z}$ direction, which is also the direction of the excitation. The sensors operate between -100 N and $+100$ N, with a precision of ± 0.5 N.

As Figure 5 shows, a force sensor is linked to the central fuel assembly, which will be noted $\mathrm{FA_{central}}$ and the corresponding measured force will be noted $f_{\mathrm{central}}(t)$. A second force sensor is linked to a fuel assembly aligned with the central fuel assembly considering the excitation direction ($\mathbf{e_z}$). This fuel assembly will be noted $\mathrm{FA_{aligned}}$ and the corresponding measured force will be noted $f_{\mathrm{aligned}}(t)$. The third force sensor is linked to a fuel assembly aligned with the central fuel assembly, but this time, in the $\mathbf{e_y}$ direction, which is transversal to the direction of excitation. This fuel assembly will be noted $\mathrm{FA_{transversal}}$ and the corresponding measured force will be noted $f_{\mathrm{transversal}}(t)$. And finally the

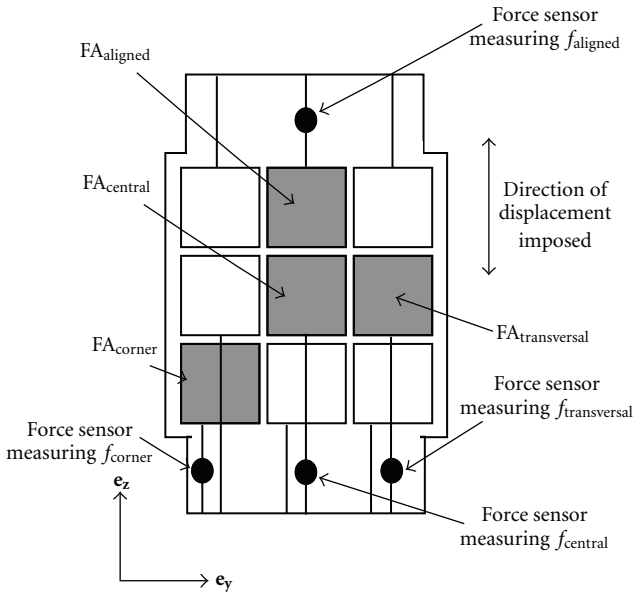

Figure 4: Force sensors disposition.

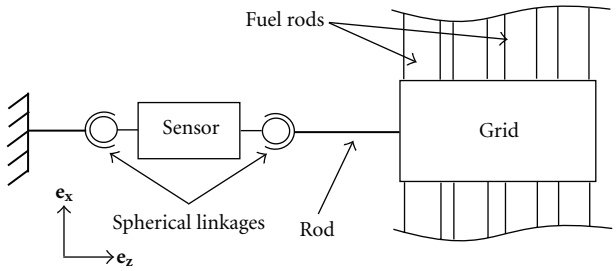

Figure 5: Force sensor.

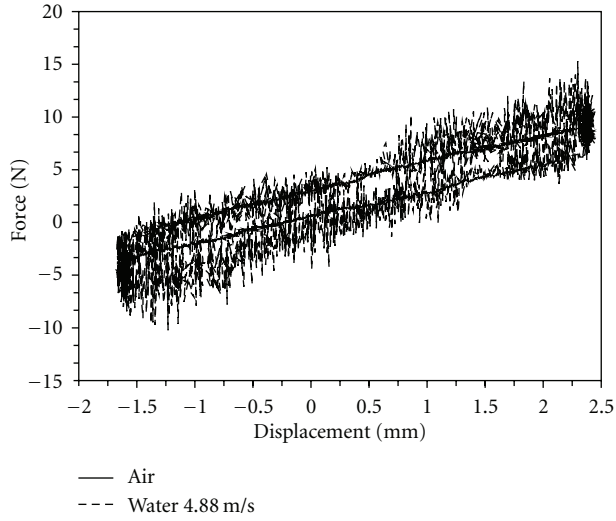

Figure 6: Force measured by the sensor 4 versus the hydraulic jack displacement, quasistatic test.

fourth force sensor is linked to a fuel assembly located at a corner. This fuel assembly will be noted FA_{corner} and the corresponding measured force will be noted $f_{corner}(t)$.

A flow meter, upstream from the test section, gives us access to the fluid velocity.

2.4. Limitations. The experimental apparatus presents some limitations that are listed in the following.

First, the friction force between the fastening rod linked to $FA_{central}$, where the motion is imposed, and the fuel assembly that it crosses, which is motionless, induces a perturbation in the measurement of the force $f_{central}(t)$, which results in the increase of the measured damping. However, the friction force does not depend on fluid flow conditions, thus, we can observe the influence of fluid flow on $f_{central}(t)$.

Secondly, each fuel assembly contains 16 rods, which is far from the 289 rods of a fuel assembly in a PWR. Moreover, the pure fluid zone, that is, the gap between the fuel assemblies, represents around 10% of the total volume, whereas in a PWR this part is less than 1%. The apparatus is less homogeneous than a PWR, which means that the flow distribution in the fuel assemblies is not the same. Since it is more difficult for the fluid to flow through a narrow channel than in a large one, the fluid velocity is higher in the channel gap than in the fuel assemblies, whereas the flow in a PWR is homogeneous because the gap has almost the same value as the distance between two rods of a fuel assembly. Thus, the coupling between fuel assemblies in the present apparatus may be different from what it is in a PWR. However, the aim of the present work is not to provide a precise value of the coupling, but to show if it is negligible or not.

Finally, locations and directions of sensors give us restricted data of the coupling forces. We have neither access to the distribution of the coupling forces along the fuel assemblies nor to the value of these forces in the transversal direction ($\mathbf{e_y}$). Such data would be useful to better understand the physical phenomenon, but for cost and implementation reasons we choose restricted data. Nevertheless, the data presented in the present study provides some interesting information.

3. Experimental Observations

3.1. Quasistatic Tests. The quasistatic tests were conducted in-air, still water, and under axial flow, to characterize the stiffness of $FA_{central}$ by measuring the force $f_{central}(t)$ and imposing the displacement $u_{central}(t)$.

In the in-air test (Figure 6, continuous line), we clearly see a phenomenon of hysteresis, with two parallel curves. This is due to the friction between the fastening rod and the fuel assembly it crosses. It appears, however, that the stiffness of the fuel assembly is linear, the slope gives us the value of that stiffness and the distance between the two curves corresponds to two times the value of the friction force.

The still water test is similar to the air test. This was expected with such low velocity excitation.

The tests under axial flow are very noisy as can be seen in Figure 6, (dashed line). The noise is certainly due to a turbulence effect. We therefore have to separate the effect of

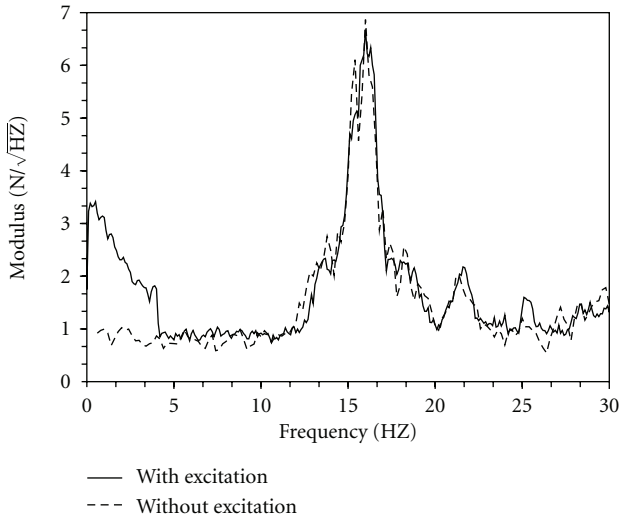

Figure 7: Square root of the autospectral density of f_{aligned} versus frequency of with and without dynamic excitation, for a 4.2 m/s fluid velocity.

turbulence from the coupling forces. This is discussed in the next Section.

In spite of the noise, we can observe that the flow induces a stiffening of the assembly. This appears counterintuitive at first sight. The axial flow induces an axial force that compresses the fuel assembly, and considering geometrical nonlinear effect, a compressive force induces a decrease of the stiffness until the force reaches the critical value at which the buckling occurs. Thus the stiffening is due to a pressure distribution induced by the flow.

3.2. Dynamic Tests. In this section, we present dynamic tests results in-air, in still water, and under axial flow at several flow velocities (from 0 m/s to 4.9 m/s).

We have to deal with very noisy data. In Figure 7, we can see the autospectral density of the force $f_{\text{aligned}}(t)$, for a 4.2 m/s fluid velocity, with and without dynamic excitation. We can observe that, in the part between 0 Hz and 4 Hz, spectral densities are very different in the two cases: it is flat without dynamic excitation, whereas it shows spectral component with dynamic excitation. In the second part, from 4 Hz to 30 Hz, the two spectral densities are very alike, and we can observe that the energy is concentrated around a peak of 16 Hz. This may correspond to a system natural mode excited by random turbulence excitation.

Figure 8 shows the autospectral density of the force $f_{\text{aligned}}(t)$, the autospectral density of the displacement imposed $u_{\text{central}}(t)$, and the coherence between $f_{\text{aligned}}(t)$ and $u_{\text{central}}(t)$. We can see that, the coherence is very close to 1 between 0 Hz and 4 Hz and has a much lower value for frequencies higher than 4 Hz. Since the band 0 Hz-4 Hz corresponds to the excited frequencies, as the spectral density of $u_{\text{central}}(t)$ shows, the spectral density of $f_{\text{aligned}}(t)$ between 0 Hz and 4 Hz characterizes the effect of $\text{FA}_{\text{central}}$ displacement on fluid forces acting on $\text{FA}_{\text{aligned}}$, that is, the coupling between $\text{FA}_{\text{central}}$ and $\text{FA}_{\text{aligned}}$.

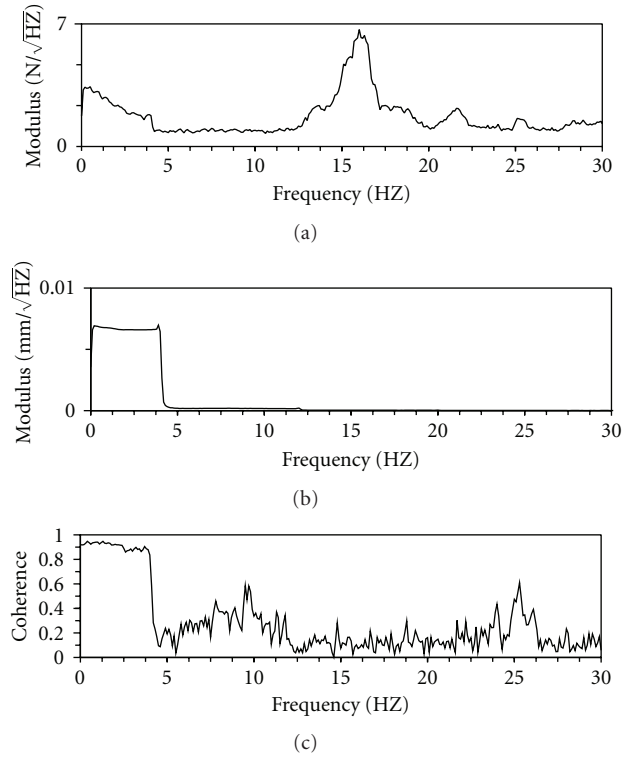

Figure 8: Square root of the autospectral density of f_{aligned} versus frequency (a); square root of the autospectral density of u_{central} versus frequency (b); coherence between f_{aligned} and u_{central} versus frequency (c); for a 4.2 m/s fluid velocity.

Figure 9 shows the transfer function between the imposed displacement $u_{\text{central}}(t)$ and the measured force $f_{\text{central}}(t)$, for in-air, in-water, and under axial flow tests. The transfer function $H_{\text{central}}(\omega)$ is calculated from the autospectral density of $f_{\text{central}}(t)$ (noted $\text{CSD}(f_{\text{central}}, f_{\text{central}})$), and the cross-spectral density (CSD) of $u_{\text{central}}(t)$ and $f_{\text{central}}(t)$ ($\text{CSD}(f_{\text{central}}, u_{\text{central}})$) as

$$H_{\text{central}}(\omega) = \frac{\text{CSD}(f_{\text{central}}, u_{\text{central}})}{\text{CSD}(f_{\text{central}}, f_{\text{central}})}. \tag{2}$$

$H_{\text{central}}(\omega)$ characterizes the mechanical behaviour of $\text{FA}_{\text{central}}$. The in-air test shows a peak at 2.5 Hz which corresponds to the natural frequency of the fuel assembly. We observe that the presence of fluid (still water test) induces an added mass effect, and a fluid damping, since, in this case, the peak is at 2.3 Hz and lower than in the air case. The flow increases the damping as the fluid velocity increases. These effects are well known and have already been observed on PWR fuel assemblies [8]. The value of the transfer function at 0 Hz corresponds to the inverse of the stiffness of $\text{FA}_{\text{central}}$. It appears, as we saw in the quasistatic test, that the flow induces a stiffening as the fluid velocity increases.

Figure 10 shows the transfer function between the imposed displacement $u_{\text{central}}(t)$ and the measured force $f_{\text{aligned}}(t)$, for in-air, in-water, and under axial flow tests. The transfer function $H_{\text{aligned}}(\omega)$ is calculated from the

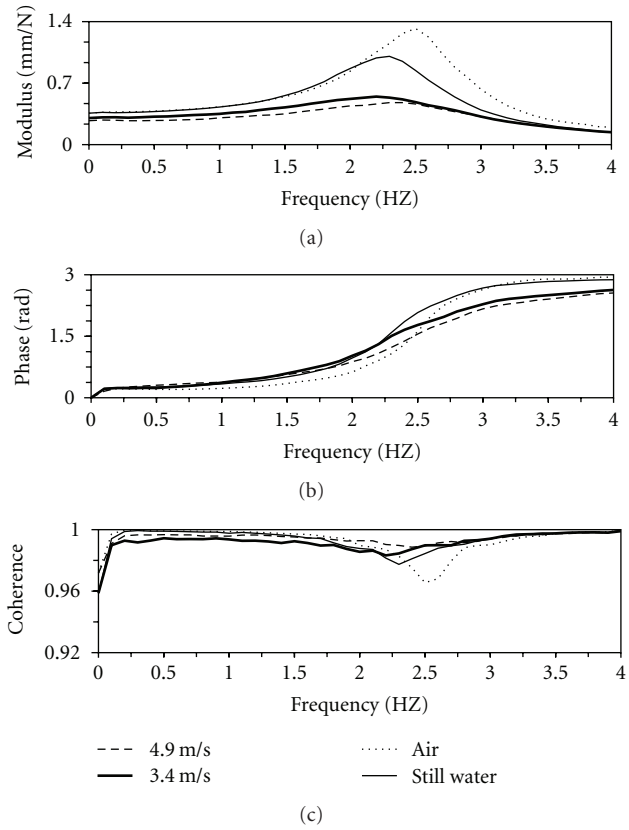

FIGURE 9: Transfer function $H_{\text{central}}(\omega)$; modulus versus frequency (a), phase versus frequency (b); coherence between f_{central} and u_{central} versus frequency (c); in-air, in still water, and for 3.4 m/s and 4.9 m/s fluid velocities.

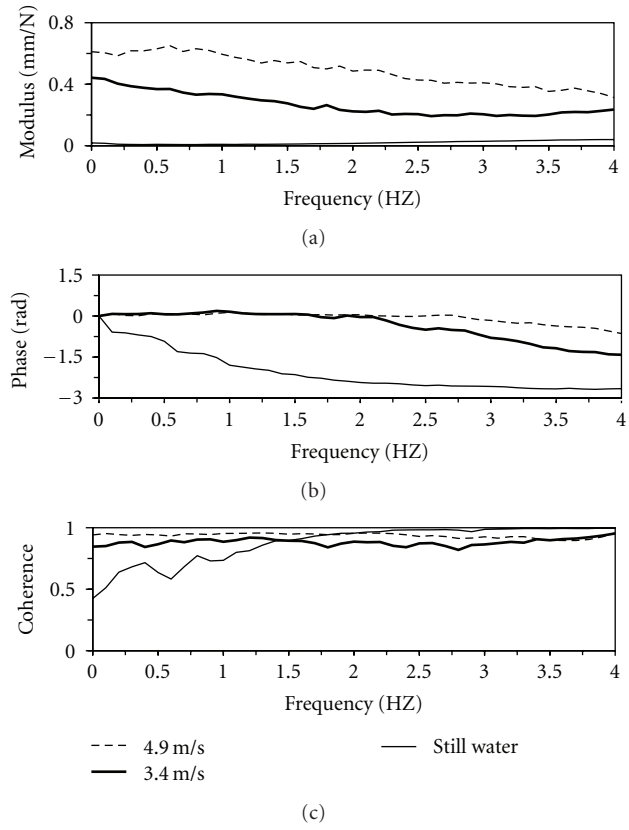

FIGURE 10: Transfer function $H_{\text{aligned}}(\omega)$; modulus versus frequency (a), phase versus frequency (b); coherence between f_{aligned} and u_{central} versus frequency (c); in still water, and for 3.4 m/s and 4.9 m/s fluid velocities.

autospectral density of $f_{\text{aligned}}(t)$, and the cross-spectral density of $u_{\text{central}}(t)$ and $f_{\text{aligned}}(t)$, as

$$H_{\text{aligned}}(\omega) = \frac{\text{CSD}\left(f_{\text{aligned}}, f_{\text{aligned}}\right)}{\text{CSD}\left(f_{\text{aligned}}, u_{\text{central}}\right)}. \tag{3}$$

Note that $H_{\text{aligned}}(\omega)$ is a complex dynamic stiffness whereas $H_{\text{central}}(\omega)$ is the inverse of a complex dynamic stiffness. $H_{\text{aligned}}(\omega)$ characterizes the coupling between $\text{FA}_{\text{central}}$ and $\text{FA}_{\text{aligned}}$, and more precisely it represents the effect of fluid forces acting on $\text{FA}_{\text{aligned}}$ induced by the displacement of $\text{FA}_{\text{central}}$. We must keep in mind that it does not characterize the mechanical behaviour of $\text{FA}_{\text{aligned}}$, since the fastening rod locks the displacement of its grid. When the modulus $|H_{\text{aligned}}(\omega)|$ reaches 0.2 N/mm, it means that a 1 mm amplitude harmonic displacement of $\text{FA}_{\text{central}}$ induces a fluid force of 0.2 N which has to be compared to the 3 N/mm stiffness of the fuel assembly. In other words, a value beyond 0.2 N/mm ($|H_{\text{aligned}}(\omega)| \geq 0.2$ N/mm) means that the coupling fluid forces have significant influence on the $\text{FA}_{\text{aligned}}$ dynamic. The high coherence value indicates that the force measured is due to the displacement of $\text{FA}_{\text{central}}$. It appears that the coupling under fluid flow is important enough, not to be neglected, whereas the coupling in still water is almost inexistent. The coupling increases with the fluid velocity, which is an expected result since the fluid damping, that is, the fluid forces, increases when the fluid velocity increases. In the axial flow case, the phase between the coupling fluid force and the $\text{FA}_{\text{central}}$ displacement remains close to 0 until 2 Hz, which indicates that the force is due to a static pressure distribution induced by the flow and the $\text{FA}_{\text{central}}$ displacement, whereas in the still water case the phase decreases which indicates that the fluid force is due to a viscous damping effect. For 3.4 m/s flow rate, the phase decreases after 2 Hz, which illustrates that the viscous damping effect starts to be more important than the static pressure distribution effect. For 4.9 m/s, the decrease of the phase occurs latter; it means that the static pressure distribution effect is depending on the flow rate.

Figure 11 shows the transfer function between the imposed displacement $u_{\text{central}}(t)$ and the measured force $f_{\text{transversal}}(t)$, for in-air, in-water, and under axial flow tests. The transfer function $H_{\text{transversal}}(\omega)$ is calculated as follows:

$$H_{\text{transversal}}(\omega) = \frac{\text{CSD}\left(f_{\text{transversal}}, f_{\text{transversal}}\right)}{\text{CSD}\left(f_{\text{transversal}}, u_{\text{central}}\right)}. \tag{4}$$

Note that $H_{\text{transversal}}(\omega)$ is a complex dynamic stiffness as $H_{\text{aligned}}(\omega)$. $H_{\text{transversal}}(\omega)$ charactcterizes the coupling between $\text{FA}_{\text{central}}$ and $\text{FA}_{\text{transversal}}$. As it is observed on the $\text{FA}_{\text{aligned}}$, the coupling is higher under axial flow than in still

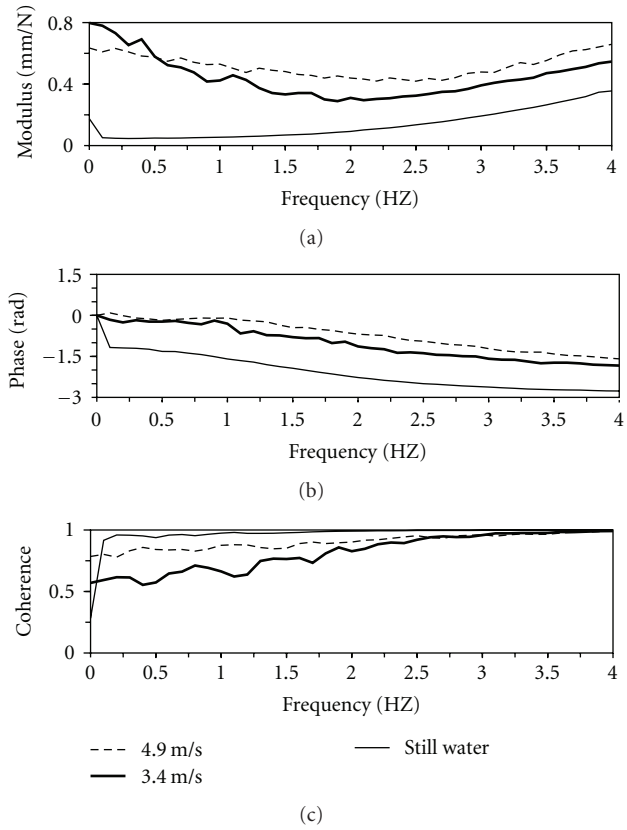

Figure 11: Transfer function $H_{\text{transversal}}(\omega)$; modulus versus frequency (a), phase versus frequency (b); coherence between $f_{\text{transversal}}$ and u_{central} versus frequency (Hz) (c); in still water, and for 3.4 m/s and 4.9 m/s fluid velocities.

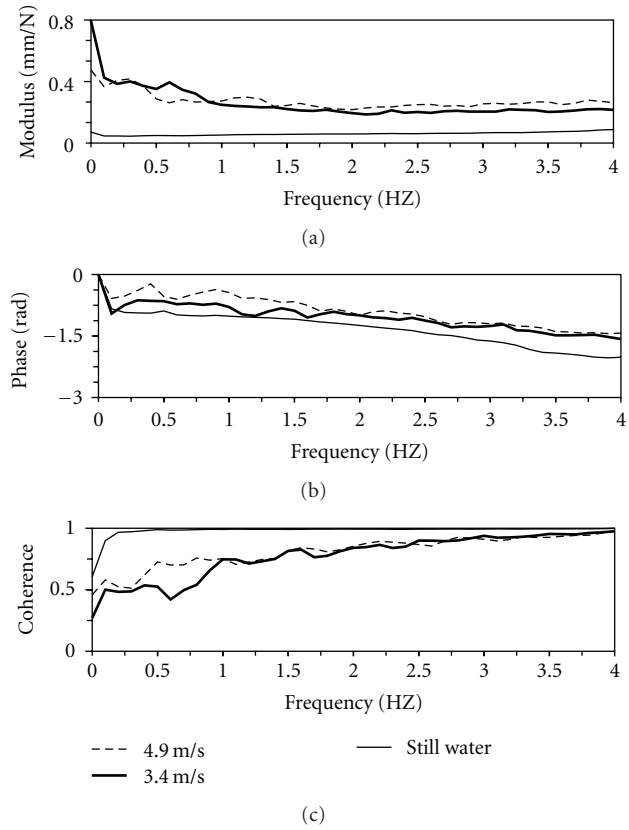

Figure 12: Transfer function $H_{\text{corner}}(\omega)$; modulus versus frequency (a), phase versus frequency (b); coherence between f_{corner} and u_{central} versus frequency (c); in still water, and for 3.4 m/s and 4.9 m/s fluid velocities.

water and its increases as the fluid velocity increases. As for $\text{FA}_{\text{aligned}}$, we observe a static pressure distribution effect at frequencies below 1 Hz induced by the $\text{FA}_{\text{central}}$ displacement. However, the phase between the force $f_{\text{aligned}}(t)$ and the $\text{FA}_{\text{central}}$ displacement decreases sooner than in the $\text{FA}_{\text{aligned}}$ case, which testify that the fluid force is mostly governed by a viscous damping effect. The static pressure distribution effect is not observed in the still water case. We can see that the modulus $|H_{\text{transversal}}(\omega)|$ reaches a value higher than 0.4 N/mm, for frequencies ranging between 3.5 Hz and 4 Hz, which means that the couplings between $\text{FA}_{\text{aligned}}$ and $\text{FA}_{\text{central}}$, and between $\text{FA}_{\text{transversal}}$ and $\text{FA}_{\text{central}}$ are comparable.

Figure 12 shows the transfer function between the imposed displacement $u_{\text{central}}(t)$ and the measured force $f_{\text{corner}}(t)$, for in-air, in-water and under axial flow tests. The transfer function $H_{\text{corner}}(\omega)$ is calculated as follows:

$$H_{\text{corner}}(\omega) = \frac{\text{CSD}(f_{\text{corner}}, f_{\text{corner}})}{\text{CSD}(f_{\text{corner}}, u_{\text{central}})}. \quad (5)$$

Note that $H_{\text{corner}}(\omega)$ is a complex dynamic stiffness as $H_{\text{aligned}}(\omega)$ and $H_{\text{transversal}}(\omega)$. $H_{\text{corner}}(\omega)$ characterize the coupling between $\text{FA}_{\text{central}}$ and $\text{FA}_{\text{corner}}$. The static pressure distribution effect is not observed on that fuel assembly, thus the coupling force is only due to a dynamic viscous damping effect due to the decrease of the phase testify. The modulus $|H_{\text{corner}}(\omega)|$ hardly reaches the value 0.2 N/mm, with a low coherence value, especially for low frequencies. We can therefore conclude that the coupling between $\text{FA}_{\text{corner}}$ and $\text{FA}_{\text{aligned}}$ is not significant and can be neglected. This result is not surprising since $\text{FA}_{\text{corner}}$ and $\text{FA}_{\text{central}}$ do not share an interface, so that the fluid flow induced by the $\text{FA}_{\text{central}}$ displacement has no significant influence on fluid forces acting on $\text{FA}_{\text{corner}}$.

4. Discussion

Two types of coupling fluid forces were observed, one is static and due to a pressure distribution induced by the flow and the other is dynamic and due to the viscous damping. The first increases with the flow rate and is not observed in still water, and its effect is more important for the $\text{FA}_{\text{aligned}}$ which is logical since the displacement of $\text{FA}_{\text{central}}$ will strongly influence the confinement of $\text{FA}_{\text{aligned}}$ and thus the fluid force acting on it. The second increases with the flow rate as well, but it is observed in the still water case. It is more important for $\text{FA}_{\text{transversal}}$.

Fluid forces acting on $\text{FA}_{\text{aligned}}$ and $\text{FA}_{\text{transversal}}$ are comparable and significant, whereas the force acting on $\text{FA}_{\text{corner}}$ seems to be negligible. The gap between fuel assemblies is larger than what can be observed in a real PWR;

therefore, the coupling between fuel assemblies should be more important than what was observed in the present study. Thus numerical simulations aiming reproduce the behaviour of a PWR core under seismic excitation should account for the 3-dimensional character of the fuel assemblies coupling. In other words, 2-dimensional simulations reproducing the behaviour of a fuel assemblies row should not be considered as representative of a PWR dynamical behaviour.

Tests were performed at room temperature (20°C) whereas a PWR works at 300°C, density ρ and viscosity μ will be different, $\rho = 1000\,\mathrm{kg}\cdot\mathrm{m}^{-3}$, and $\mu = 1002.10^6\,\mathrm{Pa}\cdot\mathrm{s}$ at 20°C, $\rho = 712\,\mathrm{kg}\cdot\mathrm{m}^{-3}$, and $\mu = 86\cdot 10^6\,\mathrm{Pa}\cdot\mathrm{s}$ at 300°C. Since the fluid forces depend on the density and the viscosity of the fluid, the coupling forces observed here should be higher than what could be found in a PWR. Nevertheless, it does not change the 3-dimensional effect.

5. Conclusion

Tests results, from an experimental apparatus involving 9 reduced-scale fuel assemblies, arranged in a 3-by-3 network and subjected to an axial flow, were presented. The displacement of the central fuel assembly was imposed while the others were fixed. The fluid forces induced by the motion of the central fuel assembly on the others were measured. We observed that the coupling between fuel assemblies increased with the fluid velocity and that the coupling in the excitation direction was comparable with the coupling in the transversal direction. Therefore, numerical modelling simulating the PWR behaviour under seismic loading should be in 3 dimensions to have accurate results. We also observed that the fluid flow induces a stiffening of the fuel assembly. Two types of coupling forces were observed, the first is due to pressure distribution, and the second is due to viscous damping.

References

[1] F. Beaud, "An analytical model for the prediction of fluidelastic forces in a rod bundle subjectedto axial flow: theory, experimental validation and application to PWR fuel assemblies," in *Proceedings of the 5th International Conference on Nuclear Engineering (ICONE '97)*, Nice, France, 1997, ICONE5-2290.

[2] E. Jacquelin, J. P. Lainé, C. Trollat, and L. Jézéquel, "Modelling the behaviour of a PWR core by a homogenization technique," *Computer Methods in Applied Mechanics and Engineering*, vol. 155, no. 1-2, pp. 1–13, 1998.

[3] E. Viallet, G. Bolsee, B. Ladouceur, T. Goubin, and J. Rigaudeau, "Validation of PWR coreseismic models with shaking table tests on interacting scale 1fuel assemblies," in *Transactions of the17th International Conference on Structural Mechanics in Reactor Technology (SMIRT '03)*, Prague, Czech Republic, 2003.

[4] R. O. Pomîrleanu, "Spectral response to harmonic excitation of rods in a confined nuclear fuelmini-bundle," in *Proceedings of the ASME Pressure Vessels and Piping Division Conference (PVP '05)*, Denver Colo, USA, 2005, paper 71486.

[5] R. J. Zhang, "Structural homogenized analysis for a nuclear reactor core," *Nuclear Engineering and Design*, vol. 183, no. 1-2, pp. 151–156, 1998.

[6] D. Broc, J. C. Queval, and E. Viallet, "Seismic behaviour of a PWR reactor core: fluid structureinteraction effects," in *Transactions of the 17th International Conference on Structural Mechanics inReactor Technology (SMIRT '03)*, Prague, Czech Republic, 2003.

[7] G. Ricciardi, S. Bellizzi, B. Collard, and B. Cochelin, "Modelling pressurized water reactor coresin terms of porous media," *Journal of Fluids and Structures*, vol. 25, no. 1, pp. 112–133, 2009.

[8] B. Collard, S. Pisapia, S. Bellizzi, and F. Witters, "PWR fuel assembly modal testing and analysis," in *Proceedings of the the ASME Pressure Vessels and Piping Conference (PVP '03)*, pp. 147–152, Cleveland, Ohio, USA, 2003.